

# A Numerical Scheme for Wave Turbulence: 3-Wave Kinetic Equations

Steven Walton and Minh-Binh Tran

Department of Mathematics  
 Southern Methodist University, Dallas, Texas 75275, USA

Email: [stevenw@mail.smu.edu](mailto:stevenw@mail.smu.edu), [minhbinht@mail.smu.edu](mailto:minhbinht@mail.smu.edu)

## Abstract

We introduce a finite volume scheme to solve isotropic 3-wave kinetic equations. We test our numerical solution against theoretical results concerning the long time behavior of the energy and observe that our solutions verify the energy cascade phenomenon. Up to our knowledge, this is the first numerical scheme that could capture the long time asymptotic behavior of solutions to isotropic 3-wave kinetic equations, where the energy cascade can be observed. Our numerical energy cascade rates are in good agreement with the theoretical one obtained by Soffer-Tran in [47]. Our finite volume algorithm relies on a new identity, that allows one to reduce the number of terms needed to be approximated in the collision operators.

## Contents

<b>1</b>	<b>Introduction</b>	<b>2</b>
<b>2</b>	<b>Comparison with Smoluchowski Coagulation Equation and a new Energy Identity</b>	<b>5</b>
<b>3</b>	<b>Finite Volume Scheme</b>	<b>7</b>
<b>4</b>	<b>Numerical Tests</b>	<b>11</b>
4.1	Test 1	11
4.2	Test 2	12
4.3	Test 3	13
4.4	Test 4	13
<b>5</b>	<b>Conclusions and Further Discussion</b>	<b>14</b>

# 1 Introduction

Over more than 60 years, the theory of weak wave turbulence has been intensively developed. Having the origin in the works of Peierls [41, 42] and the modern developments have the origin in the works of Hasselman [28, 29], Benney and Saffmann [5], Kadomtsev [33], Zakharov [53], Benney and Newell [4], wave turbulence kinetic equation equations have been shown to play important roles in a vast range of physical applications. Well known examples are water surface gravity and capillary waves, internal waves on density stratification and inertial waves due to rotation in planetary atmospheres and oceans, waves on quantized vortex lines in super fluid helium, planetary Rossby waves for the weather and climate evolutions. In rigorously deriving wave turbulence kinetic equations, Lukkarinen and Spohn are pioneers with the work [37].

In addition, to tackle the long standing open conjecture about the long time behavior of high Sobolev norms  $H^s$  ( $s > 1$ ) of solutions of dispersive equations on the torus, discussed in the works of Bourgain [1] and Colliander, Staffilani, Keel, Takaoka, Tao [8], the rigorous justification of wave turbulence theory has been revisited during the last few years in [2, 6, 7, 9, 10, 15, 16, 17, 18, 19, 20, 22, 26, 27, 48].

The 3-wave kinetic equation, one of the most important classes of wave kinetic equations, reads (see [44, 45, 51, 52, 54])

$$\begin{aligned}\partial_t f(t, p) &= \mathcal{Q}[f](t, p), \\ f(0, p) &= f_0(p),\end{aligned}\tag{1}$$

in which  $f(t, p)$  is the nonnegative wave density at wavenumber  $p \in \mathbb{R}^N$ ,  $N \geq 2$ ;  $f_0(p)$  is the initial condition. The quantity  $\mathcal{Q}[f]$  describes pure resonance and is of the form

$$\mathcal{Q}[f](p) = \iint_{\mathbb{R}^{2N}} [\mathcal{R}_{p, p_1, p_2}[f] - \mathcal{R}_{p_1, p, p_2}[f] - \mathcal{R}_{p_2, p, p_1}[f]] d^N p_1 d^N p_2 \tag{2}$$

with

$$\mathcal{R}_{p, p_1, p_2}[f] := |V_{p, p_1, p_2}|^2 \delta(p - p_1 - p_2) \delta(\omega - \omega_1 - \omega_2) (f_1 f_2 - f f_1 - f f_2)$$

with the short-hand notation  $f = f(t, p)$ ,  $\omega = \omega(p)$  and  $f_j = f(t, p_j)$ ,  $\omega_j = \omega(p_j)$ , for wavenumbers  $p, p_j, j \in \{1, 2\}$ . The function  $\omega(p)$  is the dispersion relation of the waves. The 3-wave kinetic equation has a variety of applications for ocean waves, acoustic waves, gravity capillary waves, Bose-Einstein condensate and many others (see [28, 29, 43, 50, 51, 52] and references therein).

In the isotropic case, we identify  $f(t, p)$  with  $f(t, \omega)$ , the isotropic 3-wave kinetic equation takes the form

$$\begin{aligned}\partial_t f(t, \omega) &= Q[f](t, \omega), \quad \omega \in \mathbb{R}_+, \\ f(0, p) &= f_0(p), \\ Q[f](t, \omega) &= \int_0^\infty \int_0^\infty [R(\omega, \omega_1, \omega_2) - R(\omega_1, \omega, \omega_2) - R(\omega_2, \omega_1, \omega)] d\omega_1 d\omega_2, \\ R(\omega, \omega_1, \omega_2) &:= \delta(\omega - \omega_1 - \omega_2) [U(\omega_1, \omega_2) f_1 f_2 - U(\omega, \omega_1) f f_1 - U(\omega, \omega_2) f f_2],\end{aligned}\tag{3}$$

where  $U$  satisfies  $|U(\omega_1, \omega_2)| = (\omega_1 \omega_2)^{\gamma/2}$ .

One of the breakthrough results of the weak turbulence theory ( see [35, 52, 53]) concerns the existence of the so-called Kolmogorov-Zakharov (KZ) spectra, which is a class of *time-independent solutions*  $f_\infty$  of equation (1):

$$f_\infty(p) \approx C|p|^{-\kappa}, \quad \kappa > 0,$$

which are the analogs of the Kolmogorov energy spectrum of hydrodynamic turbulence. Works on this research line have been actively continued to the present (see, for instance [24, 38, 39], to name only a few).

Up to our knowledge, relatively little has been done on the time-dependent solutions of (1). In the important works [11, 12, 13], several numerical experiments were designed, to investigate the isotropic 3-wave equation. In the work [11], it has been pointed out that isotropic 3-wave kinetic equation is equivalent to the mean field rate equations for an aggregation-fragmentation problem, which possesses an unusual fragmentation mechanism. A numerical method for solving isotropic 3-wave kinetic equation under the presence of forcing and dissipation was also introduced. In [47], Soffer and Tran show that, the solutions of (3), with  $\gamma = 2$ , exhibit the property that the energy is cascaded from small wavenumbers to large wavenumbers. They show that starting with a regular initial condition whose energy at the infinity wave number  $\omega = \infty$  is 0, as time evolves, the energy is gradually accumulated at  $\{\omega = \infty\}$ . In the long time limit, all the energy of the system is concentrated at  $\{\omega = \infty\}$  and the energy function becomes a Dirac function at infinity  $\mathcal{E}\delta_{\{\omega=\infty\}}$ , where  $\mathcal{E}$  is the total energy. To be more precise, let us define the energy of the solution (3) as  $g(t, \omega) = \omega f(t, \omega)$ . It has been proved in [47] that  $g$  can be decomposed into two parts

$$g(t, \omega) = \bar{g}(t, \omega) + \tilde{g}(t)\delta_{\omega=\infty}, \quad (4)$$

where  $\bar{g}(t, \omega) \geq 0$  is the regular part, which is a function, and  $\tilde{g}(t)\delta_{\omega=\infty}$ , is the singular part, which is a measure. The function  $\tilde{g}(t)$  is non-negative. Initially,  $\bar{g}(0, \omega) = g(0, \omega)$  and  $\tilde{g}(0) = 0$ . There exists a time  $t_0$ , such that for all time  $t > t_0$ , the function  $\tilde{g}(t)$  is strictly positive. Moreover, starting from time  $t_0$ , the energy starts to transfer from the regular part  $\bar{g}(t, \omega)$  to the singular part  $\tilde{g}(t)\delta_{\omega=\infty}$ , while the total energy of the two regular and singular parts is still conserved. In the limit that  $t \rightarrow \infty$ , all of the energy will be accumulated to the singular part. This means if we look for a strong (non-measured) solution, whose energy is conserved, it can only exist up to a very short time  $t = t_0$ , which we call the “singular behavior” time.

We refer to [47] for a detailed comparison between the different results of [11, 12, 13, 47]. Note that the energy cascade phenomenon has also been observed for the 4-wave kinetic equation, in the previous work of Escobedo and Velazquez [21]. Let us also mention the work [46], where a 3-wave kinetic equation, derived from the elastic beam wave equation on the lattice, has been analyzed. It has been shown that the domain of integration of the 3-wave collision operator is broken into disconnected domains, each has their own local equilibrium. If one starts with any initial condition, whose energy is finite on one subdomain, the solutions will relax to the local equilibrium of this subregion, as time evolves. This is the so-called non-ergodicity phenomenon, which is different from the energy cascade phenomenon observed in our current work. The global existence of 3-wave kinetic equations in the presence of

forcing has been done in [25, 40] and a connection to chemical reaction networks has also been pointed out in [49].

Starting from (3), we could rewrite the 3-wave kinetic equation under the following equivalent form

$$\begin{aligned}\partial_t f(t, k) &= \mathbb{Q}[f](t, k), \quad k \in \mathbb{R}_+, \\ f(0, k) &= f_0(k),\end{aligned}\tag{5}$$

in which  $\mathbb{Q}$  is a non-local operator of kinetic type:

$$\begin{aligned}\mathbb{Q}[f](t, k) &= \int_0^k [a(k_1, k - k_1)f(k_1)f(k - k_1) - a(k, k_1)f(k)f(k_1) \\ &\quad - a(k, k - k_1)f(k)f(k - k_1)]dk_1 \\ &\quad - 2 \int_0^\infty [a(k, k_1)f(k)f(k_1) - a(k + k_1, k_1)f(k + k_1)f(k_1) \\ &\quad - a(k_1, k)f(k)f(k_1)]dk_1,\end{aligned}\tag{6}$$

where the collision kernel satisfies  $a(k_1, k_2) = (k_1 k_2)^{\gamma/2}$ . Note  $k$  is simply  $\omega$  multiplied by a fixed constant.

The goal of our paper is then to derive a finite volume algorithm that allows us to observe the time evolution of the solutions of (5) and to verify the theoretical results of [47] for various values of  $\gamma$ . In other words, we aim to observe the transferring of energy from the regular to the singular parts in (4), after the “singular behavior” time  $t_0$  discussed above, as well as to measure precisely the rate of this process, that we call the energy cascade rate.

Our finite volume scheme relies on the combination of a new energy identity represented in Lemma 2.1 and an adaptation of Filbet-Laurençot’s scheme [23] for the Smoluchowski coagulation equation to the 3-wave kinetic equation. Most numerical schemes that approximate integrals on unbounded domains require the truncation of the unbounded domains to finite domains. Thanks to the new identity, the number of terms in the collision operators is reduced, and thus, the number of truncation needed for the collision operator is also reduced. We will see later that the truncation of the terms in the collision operator really affects the accuracy of the numerical scheme, thus the reduction the number of terms make the scheme more accurate and reliable. Indeed, we only need to truncate twice in our numerical scheme.

**Acknowledgment:** The authors are funded in part by the NSF RTG Grant DMS-1840260, NSF Grant DMS-1854453, URC Grant 2020, Humboldt Fellowship, Dedman College Linking Fellowship, NSF CAREER DMS-2044626. They would like to thank Prof. T. Hagstrom for the use of SMU’s high-performance compute cluster ManeFrame II (M2) and Prof. S. Nazarenko and Prof. B. Rumpf for several constructive suggestions to improve numerical plots.

## 2 Comparison with Smoluchowski Coagulation Equation and a new Energy Identity

In [23], Filbet and Laurençot derive a finite volume scheme (FVS) for the Smoluchowski coagulation equation (SCE)

$$\begin{aligned}\partial_t f(t, k) &= \mathbb{Q}_{Smo}[f](t, k), \\ f(0, k) &= f_0(k),\end{aligned}\tag{7}$$

$$\mathbb{Q}_{Smo}[f](t, k) = \int_0^k a(k_1, k - k_1) f(k_1) f(k - k_1) dk_1 - 2 \int_0^\infty a(k, k_1) f(k) f(k_1) dk_1,\tag{8}$$

where  $a(\cdot, \cdot)$  is the collision kernel for the 3-wave collision operator (6). Let us give a short derivation of the non-conservative form of the SCE (see [3], [14], [23] and the references therein).

Take a test function  $\phi(k) = k$  and apply it to the SCE

$$\begin{aligned}\int_0^c \partial_t f(t, k) k dk &= \int_0^c \int_0^k a(k, k - k_1) f(k_1) f(k - k_1) k dk_1 dk \\ &\quad - 2 \int_0^c \int_0^\infty a(k, k_1) f(k) f(k_1) k dk_1 dk \\ &= 2 \int_0^c \int_0^{c-k} a(k, k_1) f(k) f(k_1) k dk_1 dk - 2 \int_0^c \int_0^\infty a(k, k_1) f(k) f(k_1) k dk_1 dk.\end{aligned}$$

Rearranging the right-hand side, we find

$$\int_0^c \partial_t f(t, k) k dk = -2 \int_0^c \int_{c-k}^\infty a(k, k_1) f(k_1) f(k) k dk_1 dk,$$

and upon taking the derivative with respect to  $c$ ,

$$\partial_t f(t, c) c = -2 \partial_c \int_0^c \int_{c-k}^\infty a(k, k_1) f(k_1) f(k) k dk_1 dk,$$

and truncating the inner integral,

$$\partial_t f(t, c) c = -2 \partial_c \int_0^c \int_{c-k}^R a(k, k_1) f(k_1) f(k) k dk_1 dk,\tag{9}$$

where  $R$  is a suitable truncation of the volume. Then one can apply any finite volume scheme to solve the truncated problem. We note briefly that the choice of  $R$  can effect the accuracy and efficiency of the scheme for the SCE. For example, when considering the case of gelation,  $R$  must be quite large in order to avoid a loss of mass before the gelation time. Also, in [34], the authors compare the FVS above with a finite element approximation and find that for smaller truncation values, the finite element scheme is a better choice, while for larger truncation values the FVS should be used.

If we compare equation (6) with equation (8), we see that the Smoluchowski coagulation equation is a special case of the 3-wave equation. Thus, we would like to adapt the (FVS) of

Filbet and Laurençot to derive a numerical scheme for the 3-wave equation. To do this we derive a similar identity to (9) for the wave kinetic equation. The role of this identity is to reduce the number of terms in the collision operator. As discussed above, the truncation of the terms in the collision operator can affect the accuracy of the numerical scheme, thus that the number of truncated terms is reduced is quite crucial in the numerical computations of the solutions, as it allows the scheme to be more accurate and reliable.

However, for the 3-wave equation, unlike for the SCE, the wave action,  $f(t, k)$ , is not conserved, but the energy,  $g(t, k) = f(t, k)k$ , is conserved. Further, since we do not have an analytic solution to test against, we validate our scheme by verifying some of the results for the 3-wave equation found in Soffer and Tran [47]. The results therein are concerned with the long time behaviour of the energy  $g(t, k)$  that we have just defined.

**Lemma 2.1.** *The following identity holds true for the energy function  $g(t, k)$*

$$\begin{aligned} \partial_t \frac{g(t, c)}{c} = & -2\partial_c \int_0^c \int_0^c a(k, k_1) \frac{g(k)}{k} \frac{g(k_1)}{k_1} \chi\{c < k + k_1\} dk_1 dk \\ & + \partial_c \int_0^\infty \int_0^\infty a(k, k_1) \frac{g(k)}{k} \frac{g(k_1)}{k_1} \chi\{c < k + k_1\} dk dk_1, \end{aligned} \quad (10)$$

with  $\chi\{\cdot\}$  the characteristic function and initial condition  $g(0, k) = g_0(k) = f(0, k)k$ .

*Proof.* Let  $\phi(\omega)$  be a test function. From [47], we have the following identity for the 3-wave equation

$$\int_0^\infty \partial_t f(t, k) \phi(k) dk = \int_0^\infty \int_0^\infty a(k, k_1) f(k) f(k_1) [\phi(k+k_1) + \phi(|k-k_1|) - 2\phi(\max\{k, k_1\})] dk dk_1. \quad (11)$$

If we choose  $\phi(k) = \chi_{[0, c]}(k)$  (compare this with  $\phi(k) = k\chi_{[0, c]}(k)$  in [23]), we have

$$\int_0^\infty \partial_t f(t, k) \chi_{[0, c]}(k) dk = \int_0^\infty \int_0^\infty a(k, k_1) f(k) f(k_1) [\chi_{[0, c]}(k+k_1) + \chi_{[0, c]}(|k-k_1|) - 2\chi_{[0, c]}(\max\{k, k_1\})] dk dk_1. \quad (12)$$

Set  $K(k, k_1) = \chi_{[0, c]}(k+k_1) + \chi_{[0, c]}(|k-k_1|) - 2\chi_{[0, c]}(\max\{k, k_1\})$ . There are seven cases:

- i Assume  $k + k_1 \leq c$  then we have  $\chi_{[0, c]}(k+k_1) = 1$ ,  $\chi_{[0, c]}(|k-k_1|) = 1$  and  $\chi_{[0, c]}(\max\{k, k_1\}) = 1$  which implies that  $K(k, k_1) = 0$ .
- ii Assume that  $k + k_1 > c$  but  $k \leq c$  and  $k_1 \leq c$  Then we have  $\chi_{[0, c]}(k+k_1) = 0$ ,  $\chi_{[0, c]}(|k-k_1|) = 1$ ,  $\chi_{[0, c]}(\max\{k, k_1\}) = 1$  and so  $K(k, k_1) = -1$ .
- iii Now let  $k + k_1 > c$ ,  $k \leq c$  but  $k_1 > c$  then  $\chi_{[0, c]}(k+k_1) = 0$ ,  $\chi_{[0, c]}(|k-k_1|) = 1$ , and  $\chi_{[0, c]}(\max\{k, k_1\}) = 0$  giving  $K(k, k_1) = 1$ .
- iv Assume  $k + k_1 > c$ , with  $k > c$  and  $k_1 \leq c$  and  $|k-k_1| > c$ , then  $\chi_{[0, c]}(k+k_1) = 0$ ,  $\chi_{[0, c]}(|k-k_1|) = 0$ ,  $\chi_{[0, c]}(\max\{k, k_1\}) = 0$  leaving  $K(k, k_1) = 0$ .
- v Assume  $k + k_1 > c$ , with  $k > c$  and  $k_1 \leq c$  and  $|k-k_1| \leq c$ , then  $\chi_{[0, c]}(k+k_1) = 0$ ,  $\chi_{[0, c]}(|k-k_1|) = 1$ ,  $\chi_{[0, c]}(\max\{k, k_1\}) = 0$  leaving  $K(k, k_1) = 1$ .

vi Lastly, set  $k + k_1 > c$ ,  $k > c$ ,  $k_1 > c$ , and  $|k - k_1| > c$ , then  $\chi_{[0,c]}(k + k_1) = 0$ ,  $\chi_{[0,c]}(|k - k_1|) = 0$  and  $\chi_{[0,c]}(\max\{k, k_1\}) = 0$  resulting in  $K(k, k_1) = 0$ .

vii Lastly, set  $k + k_1 > c$ ,  $k > c$ ,  $k_1 > c$ , and  $|k - k_1| \leq c$ , then  $\chi_{[0,c]}(k + k_1) = 0$ ,  $\chi_{[0,c]}(|k - k_1|) = 1$  and  $\chi_{[0,c]}(\max\{k, k_1\}) = 0$  resulting in  $K(k, k_1) = 1$ .

Applying these computations to (12) and after taking the derivative as done for (9), we have

$$\begin{aligned} \partial_t f(t, c) &= -\partial_c \int_0^\infty \int_0^\infty a(k, k_1) f(k) f(k_1) \chi\{c < k + k_1\} \chi\{k \wedge k_1 \leq c\} dk_1 dk \\ &\quad + \partial_c \int_0^\infty \int_0^\infty a(k, k_1) f(k) f(k_1) \chi\{c < k + k_1\} \chi\{k \wedge k_1 > c\} dk dk_1, \end{aligned} \quad (13)$$

which gives

$$\begin{aligned} \partial_t f(t, c) &= -2\partial_c \int_0^c \int_0^c a(k, k_1) f(k) f(k_1) \chi\{c < k + k_1\} dk_1 dk \\ &\quad + \partial_c \int_0^\infty \int_0^\infty a(k, k_1) f(k) f(k_1) k_1 \chi\{c < k + k_1\} dk dk_1, \end{aligned} \quad (14)$$

which yields (10).  $\square$

With the identity (10) in hand, we now derive a finite volume scheme with which to solve it. Note that with (10), we only need to truncate the integral  $\int_0^\infty$  twice, while with the original formula (6), we are required to truncate three terms. However, as will be seen in the next section, for a uniform grid we may greatly simplify the approximation to 10 thanks to the characteristic functions in the integrands.

### 3 Finite Volume Scheme

We give a discretization for the frequency domain for  $k \in [0, R]$ , Let  $i \in \{0, 1, 2, \dots, M\} = I_h^M$ , with  $h \in (0, 1)$  fixed and  $M = M(h)$ . Then, we define the set  $S_d = \{0, \dots, R\}$  to be the discretization of the interval  $[0, R]$ . Let

$$S_d = \{k_{i+1/2}\}_{i \in I_h^M}, \quad \{k_i\}_{i \in I_h^M \setminus \{0\}} = \frac{k_{i+1/2} + k_{i-1/2}}{2}, \quad \{\Delta k_i\}_{i \in I_h^M \setminus \{0\}} = k_{i+1/2} - k_{i-1/2} \leq h,$$

define the faces, pivots and step-size respectively, with  $k_{1/2} = 0$  and  $k_{M+1/2} = R$ . Note that the discretization does not require a uniform grid, but does restrict the step-size. The set  $T_N = \{0, \dots, T\}$  with  $N + 1$  nodes, where  $T$  is the maximum time, is the discretization of the time domain. We fix the time step to be  $\Delta t = \frac{T}{N}$ , and denote by  $t_n = \Delta t \cdot n$  for  $n \in \{0, \dots, N\}$ . We approximate equation (10) with

$$g^{n+1}(k_i) = g^n(k_i) + \lambda_i \left( Q_{i+1/2}^n \left[ \frac{g}{k} \right] - Q_{i-1/2}^n \left[ \frac{g}{k} \right] \right), \quad (15)$$

where  $\lambda_i = \frac{k_i \Delta t}{\Delta k_i}$ , and

$$Q_{i+1/2}^n \left[ \frac{g}{k} \right] - Q_{i-1/2}^n \left[ \frac{g}{k} \right] = -2 \left( Q_{1,i+1/2}^n \left[ \frac{g}{k} \right] - Q_{1,i-1/2}^n \left[ \frac{g}{k} \right] \right) + \left( Q_{2,i+1/2}^n \left[ \frac{g}{k} \right] - Q_{2,i-1/2}^n \left[ \frac{g}{k} \right] \right),$$

with

$$Q_{1,i+1/2}^n \left[ \frac{g}{k} \right] = \sum_{m=0}^i \Delta k_m \frac{g^n(k_m)}{k_m} \left( \sum_{j=0}^i \Delta k_j \frac{g^n(k_j)}{k_j} a(k_m, k_j) \chi \left\{ k_{i+1/2} < k_m + k_j \right\} \right), \quad (16)$$

$$Q_{2,i+1/2}^n \left[ \frac{g}{k} \right] = \sum_{m=0}^M \Delta k_m \frac{g^n(k_m)}{k_m} \left( \sum_{j=0}^M \Delta k_j \frac{g^n(k_j)}{k_j} a(k_m, k_j) \chi \left\{ k_{i+1/2} < k_m + k_j \right\} \right), \quad (17)$$

where we have used the midpoint rule to approximate the integrals in equation (10) and we choose an explicit time stepping method.

We will be interested in computing the moments of our solution. We approximate the  $\ell$ -th moment,  $\mathcal{M}^\ell(t_n)$ , by

$$\mathcal{M}^\ell(t_n) = \sum_{i=0}^M \Delta k_i g^n(k_i) k_i^\ell, \quad (18)$$

with  $\ell \in \mathbb{N}$ .

The initial condition  $g_0(k)$  is approximated by

$$g^0(k_i) = \frac{1}{\Delta k_i} \int_{k_{i-1/2}}^{k_{i+1/2}} g_0(k) dk \approx g_0(k_i),$$

by again employing the midpoint rule. We have that  $g^0(k_i) \geq 0$  for all  $i \in \{1, \dots, M\}$  since  $g_0(k) \geq 0$  for all  $k \in [0, R]$  by assumption. To ease notation in the proof of the following proposition, we write  $g_i^n$  for  $g^n(k_i)$  and

$$\delta Q_{1,i}^n \left[ \frac{g}{k} \right] = Q_{1,i+1/2}^n \left[ \frac{g}{k} \right] - Q_{1,i-1/2}^n \left[ \frac{g}{k} \right] \quad (19)$$

and

$$\delta Q_{2,i}^n \left[ \frac{g}{k} \right] = Q_{2,i+1/2}^n \left[ \frac{g}{k} \right] - Q_{2,i-1/2}^n \left[ \frac{g}{k} \right] \quad (20)$$

for the flux terms, so that

$$\delta Q_i^n \left[ \frac{g}{k} \right] = \delta Q_{2,i}^n \left[ \frac{g}{k} \right] - 2 \delta Q_{1,i}^n \left[ \frac{g}{k} \right].$$

Let us now assume that we have a uniform grid. Then

$$S_d = \{ih\}_{i \in I_h^M}, \quad \{k_i\}_{i \in I_h^M \setminus \{0\}} = \frac{h}{2}(2i-1), \quad \{\Delta k_i\}_{i \in I_h^M \setminus \{0\}} = h \in (0, 1),$$

and our approximations may be simplified as follows:

$$\begin{aligned}
\delta Q_{1,i}^n \left[ \frac{g}{k} \right] &= -2^{2-\gamma} h^\gamma \left[ \sum_{m=1}^i \frac{g_m^n}{2m-1} \sum_{r=0}^i \frac{g_r^n}{2r-1} ((2r-1)(2m-1))^{\gamma/2} \chi\{i+1 < m+r\} \right. \\
&\quad \left. - \sum_{m=1}^{i-1} \frac{g_m^n}{2m-1} \sum_{r=1}^{i-1} \frac{g_r^n}{2r-1} ((2r-1)(2m-1))^{\gamma/2} \chi\{i < m+r\} \right] \\
&= -2^{2-\gamma} h^\gamma \left[ \frac{(g_i^n)^2}{(2i-1)^{2-\gamma}} + \frac{2g_i^n}{(2i-1)^{1-\gamma/2}} \sum_{m=1}^{i-1} \frac{g_m^n}{2m-1} (2m-1)^{\gamma/2} \chi\{i+1 < i+m\} \right. \\
&\quad + \sum_{m=1}^{i-1} \frac{g_m^n}{2m-1} \sum_{r=1}^{i-1} \frac{g_r^n}{2r-1} ((2m-1)(2r-1))^{\gamma/2} \chi\{i+1 < m+r\} \\
&\quad \left. - \sum_{m=1}^{i-1} \frac{g_m^n}{2m-1} \sum_{r=1}^{i-1} \frac{g_r^n}{2r-1} ((2m-1)(2r-1))^{\gamma/2} \chi\{i < m+r\} \right] \\
&= -2^{2-\gamma} h^\gamma \left[ \frac{(g_i^n)^2}{(2i-1)^{2-\gamma}} + \frac{2g_i^n}{(2i-1)^{1-\frac{\gamma}{2}}} \sum_{m=2}^{i-1} \frac{g_m^n}{2m-1} (2m-1)^{\gamma/2} \right. \\
&\quad \left. - \sum_{m=2}^{i-1} \frac{g_m^n}{2m-1} \frac{g_{i+1-m}^n}{2(i+1-m)-1} \left( (2m-1)(2(i+1-m)-1) \right)^{\gamma/2} \right], \tag{21}
\end{aligned}$$

where we used the properties of the characteristic function, made clear in the following calculation, and elementary computations. For the second term we have

$$\begin{aligned}
\delta Q_{2,i}^n \left[ \frac{g}{k} \right] &= h^\gamma 2^{2-\gamma} \left( \sum_{m=1}^M \frac{g_m^n}{2m-1} \sum_{r=1}^M \frac{g_r^n}{2r-1} ((2r-1)(2m-1))^{\gamma/2} \right. \\
&\quad \times \left. \left( \chi\{i+1 < m+r\} - \chi\{i < m+r\} \right) \right), \\
&= -h^\gamma 2^{2-\gamma} \left( \sum_{m=1}^M \frac{g_m^n}{2m-1} \sum_{r=1}^M \frac{g_r^n}{2r-1} ((2r-1)(2m-1))^{\gamma/2} \chi\{i+1 = m+r\} \right), \\
&= -h^\gamma 2^{2-\gamma} \sum_{m=1}^i \frac{g_m^n}{2m-1} \frac{g_{i+1-m}^n}{2(i+1-m)-1} \left( (2m-1)(2(i+1-m)-1) \right)^{\gamma/2}. \tag{22}
\end{aligned}$$

The following proposition introduces a restriction on the time step to ensure positivity of solutions. The result is given for a uniform grid.

**Proposition 3.1.** *If the time step is such that the following inequality is satisfied*

$$\Delta t \lesssim \frac{g_i^0 + \int_0^{t_n} \delta Q_i \left[ \frac{g}{k} \right] dt}{n^2(1-2i) \langle \delta Q_i^n \left[ \frac{g}{k} \right] \rangle_n}, \tag{23}$$

where  $\langle \cdot \rangle_n$  denotes the average over  $n$  nodes in the time domain discretization, then, for

$$g_i^{n+1} = g_i^n + \lambda_i \delta Q_i^n \left[ \frac{g}{k} \right], \tag{24}$$

we have that  $g_i^{n+1}$  is positive.

*Proof.* We can rewrite equation 24 recursively as

$$\begin{aligned}
g_i^{n+1} &= g_i^n + \lambda_i \delta Q_i^n \left[ \frac{g}{k} \right] \\
&= g_i^{n-1} + \lambda_i \delta Q_i^{n-1} \left[ \frac{g}{k} \right] + \lambda_i \delta Q_i^n \left[ \frac{g}{k} \right] \\
&\quad \vdots \\
&= g_i^0 + (n+1) \lambda_i \sum_{s=0}^n \delta Q_i^s \left[ \frac{g}{k} \right] \\
&= g_i^0 + \Delta t (n+1) (2i-1) \sum_{s=0}^n \delta Q_i^s \left[ \frac{g}{k} \right].
\end{aligned}$$

Then, we must have

$$g_i^0 \geq \Delta t (n+1) (1-2i) \sum_{s=0}^n \delta Q_i^s \left[ \frac{g}{k} \right].$$

Rewriting the right-hand side of the above, we get

$$\begin{aligned}
g_i^0 &\geq \Delta t n (1-2i) \sum_{s=0}^n \delta Q_i^s \left[ \frac{g}{k} \right] + \Delta t (1-2i) \sum_{s=0}^n \delta Q_i^s \left[ \frac{g}{k} \right] \\
&\gtrsim \Delta t n (1-2i) \sum_{s=0}^n \delta Q_i^s \left[ \frac{g}{k} \right] + (1-2i) \int_0^{t_n} \delta Q_i \left[ \frac{g}{k} \right] dt \\
&= \Delta t (1-2i) n^2 \langle \delta Q_i \left[ \frac{g}{k} \right] \rangle_n + (1-2i) \int_0^{t_n} \delta Q_i \left[ \frac{g}{k} \right] dt.
\end{aligned}$$

Rearranging, we get

$$\frac{g_i^0 + (2i-1) \int_0^{t_n} \delta Q_i \left[ \frac{g}{k} \right] dt}{(1-2i) n^2 \langle \delta Q_i \left[ \frac{g}{k} \right] \rangle_n} \gtrsim \Delta t, \quad (25)$$

which by assumption (23) holds, and implies that

$$g_i^{n+1} = g_i^0 + (n+1) \lambda_i \sum_{s=0}^n \delta Q_i^s \left[ \frac{g}{k} \right] \geq 0 \quad (26)$$

□

Evidence for the dependence of the time step on the initial condition will be seen below in the next section.

## 4 Numerical Tests

All tests were performed on a uniform grid, with  $\Delta k = 0.5$  in the first two test and  $\Delta k = 0.1$  in the last two. We solve the 3-wave equation via (10) for four different initial conditions. For each initial condition, we either vary the truncation parameter,  $R$ , and hold the degree of the collision kernel,  $\gamma$ , fixed or we vary  $\gamma$  with  $R$  kept at a fixed value. Specifically, for the first two initial condition, we run tests for  $R = 50, 100, 200$  with  $\gamma = 2$  fixed or  $\gamma = 0, 1, 2$  with  $R = 100$  fixed. In the last two cases, we do something similar and again run tests with  $\gamma = 2$  fixed but set  $R = 25, 50, 80$  and then fix  $R = 50$  and let  $\gamma = 0, 1, 2$ . In all solutions presented, we use a second-order Runge-Kutta scheme for the time-step.

The first few moments of the energy,  $g(t, k)$ , are then computed for each set of parameters. We find our numerical experiments to be in good agreement with [47]. We note that, as with explicit methods for the Smoluchowski equation, the CFL condition can be very restrictive (see [36]) if one wants to maintain positivity. Similarly to schemes for other types of kinetic equations, maintaining the positivity of the numerical solutions is also an important issue in our scheme. We provide a condition in Proposition 3.1 that guarantees the positivity of the solutions. Under this condition, the positivity can be preserved when we choose  $\Delta t$  sufficiently small. We observe the choice of  $\Delta t$  depends on the initial data and the size of the truncated interval. For example, in Test 1 we set  $\Delta t = 0.05$  and in Test 2 we set  $\Delta t = 0.005$ , though we perform computation over the same truncation parameter. Also, in Tests 3 and 4, as we increase the truncation parameter from  $R = 50$  to  $R = 80$ , we must drop the time step from  $\Delta t = 0.0004$  to  $\Delta t = 0.00025$  and  $\Delta t = 0.0004$  to  $\Delta t = 0.000285714$ , respectively.

We believe that common positive preserving techniques like those developed in [30, 31, 32] could potentially be a solution to handle this instability issue.

### 4.1 Test 1

Here we choose initial condition

$$g_0(k) = 1.26157e^{-50(k-1.5)^2} \quad (27)$$

with  $\Delta t = 0.05$  for  $t \in [0, T]$ ,  $T = 10000$  seconds, over a uniform frequency grid, as mentioned previously, with  $\Delta k = 0.5$ . The initial condition and final state,  $g(T, k)$ , are plotted in Figure 1a and 1b, respectively, for  $\gamma = 2$  and  $R = 100$ . The case  $\gamma = 2$  has already been considered theoretically in [47], in which it has been proved that as  $t$  tends to  $\infty$ , the energy  $g(t, k)$  converges to a delta function  $\delta_{k=\infty}$ . Moreover, the energy on any finite interval also goes to 0

$$\lim_{t \rightarrow \infty} g(t, k) \chi_{[0, R]}(k) = 0. \quad (28)$$

The two Figures 1a and 1b indeed give strong evidence for the theoretical result (28), proved in [47].

The first four moments of the energy are shown in Figure 2 for  $\gamma = 0, 1, 2$  and  $k \in [0, 100]$ . The numerical results in Figure 2 show that higher moments of  $g$  also decays to 0, due to (28). As mentioned above, for the zeroth moment, the blue curve corresponding to  $\gamma = 2$  is below the yellow curve for  $\gamma = 0$  and the red curve for  $\gamma = 1$ . However, for higher

moments, an interesting phenomenon happens. The yellow curve has a big jump when  $t$  is around 10 to 40 seconds, and it lies above the red and the blue curves from that time on, while the blue curve is still below the red curve at longer times. While (28) can be used to predict what happens in the two Figures 1a and 1b, the Figure 2 indeed needs a different theoretical explanation, which should be an interesting subject of analysis in a follow-up paper.

We then investigate the moments for increasing values of the truncation parameter. Thus, the first four moments of  $g(t, k)$  are plotted in Figure 3 with  $\gamma = 2$  fixed. For this initial condition, increasing the truncation parameter seems to have a negligible affect on the higher moments. For the other initial conditions in the test cases that follow, the difference is more distinguishable, though only for a very short interval of time. When we are able to make a distinction, the decay (28) seems to be slower for larger values of the truncation parameter  $R$ . This observation is consistent with the findings of [47] and can be understood as follows. As the energy moves away from the zero frequency  $k = 0$  and goes to the frequency  $k = \infty$  as time evolves, the chance of having some energy in a finite interval  $k \in [0, R]$  increases when  $R$  increases. Thus, the decay (28) is slower when  $R$  is larger. The energy cascade rate is independent of the truncation parameter  $R$  in the long time limit, as  $R$  indicates the energy that escapes from a finite region  $[0, R]$ .

Fixing  $\gamma = 2$ , we test the decay rate of the total energy in  $[0, \infty)$  obtained in [47]. In Figure 4, we plot the log of the zeroth moment of  $g(t, k)$  for truncation parameter  $R = 200$  against  $-\frac{1}{2} \log(t)$ , the log of the theoretical decay rate of the total energy in  $[0, \infty)$ . In [47], it has been shown that the decay rate can be bounded by  $\mathcal{O}(\frac{1}{\sqrt{t}})$ , which has very good agreement with the numerical results, where the slope of the decay rate curve in the long time limit are quite below the slope of the line  $-\frac{1}{2} \log(t)$ .

## 4.2 Test 2

We next choose a Gaussian further away from the origin

$$g_0(k) = (5\pi)^{-1/2} e^{-(k-50/3)^2/2.5} \quad (29)$$

as our initial condition. Solutions are computed up to  $T = 10000$  seconds with  $\Delta t = 0.005$  and  $\Delta k = 0.5$ . The initial condition and final state can be seen in Figure 5a and 5b, respectively. This test is designed based on Test 1, as we are curious to see what happens if we move the Gaussian away from zero.

In figures 5a and 5b we see that the energy is pushed slightly toward the origin at some  $T_s \in [0, T)$  to  $k = 11.75$ , away from its initial concentration at  $k = 16.667$  at  $t = 0$ . From this time  $T_s$  onward, the  $L^\infty$  norm of  $\|g(t, k)\chi_{[0, R]}(k)\|_{L^\infty}$  decreases to  $4.01^{-5}$  for  $t = 10000$ , maintaining its concentration at  $k = 11.75$ . This indicates the energy cascade phenomenon does happen and happens in a very special way. An analysis then needs to be done to explain this long time behavior of the solution.

We compute the moments of  $g(t, k)$  over the fixed interval  $[0, 100]$  for  $\gamma = 0, 1, 2$  in Figure 6. This behavior is quite the same with the behavior depicted in Figure 2 of Test 1.

The moment calculations are repeated with  $\gamma = 2$  fixed and varying truncation parameter. The results are plotted in Figure 7. In contrast to Figure 3, the difference in moments is more distinguishable and for a longer time interval than any other initial condition we

consider. However, as already mentioned, this is consistent with the previous analysis in [47], being that the chance of finding energy in a larger frequency interval is higher.

The theoretical decay rate is compared with the decay of total energy in Figure 8 with  $\gamma = 2$  and truncation parameter  $R = 200$ . As in Test 1, the numerical results have a good agreement with the theoretical findings of [47]. It appears the decay is  $\mathcal{O}(\frac{1}{t})$ , which is bounded by  $\mathcal{O}(\frac{1}{\sqrt{t}})$ . This is demonstrated in Figure 9.

### 4.3 Test 3

Here, we consider periodic initial data given by

$$g_0(k) = \begin{cases} 1 & k \in [2n\pi, (2n+1)\pi] \\ 0 & k \in ((2n+1)\pi, 2(n+1)\pi) \end{cases} \text{ for } n = 0, 1, 3, 5, \dots \quad (30)$$

and perform test for  $t \in [0, T]$  for  $T = 100$  and  $\Delta t = 0.0004$  when  $R = 25$  and  $R = 50$  and  $\Delta t = 0.00025$  for  $R = 80$ . The frequency step is  $\Delta k = 0.1$  for each interval  $[0, R]$  considered.

In Figure 10a we show the initial condition and in Figure 10b the final state at  $T = 100$  seconds. Once again, we see a decay of the energy. In the final state, it would appear that the remaining energy in the interval is collected near  $k = 0$  with decreasing maximum amplitude at  $k = 0.05$ . It seems that this profile is maintained as  $T \rightarrow \infty$ , in a similar fashion to Tests 1 and 2.

In Figure 11, we show the total energy while varying the degree  $\gamma$  as before. This test is in agreement with the previous test cases, in that we have a slower decay initially for smaller values of  $\gamma$ . This result differs somewhat from the same example in the other test cases in that we have a small interval of time where the decay rate of energy corresponding to  $\gamma = 2$  is surpassed by the rate corresponding to  $\gamma = 1$  and then  $\gamma = 0$ . The rates then converge as time evolves.

We then vary the truncation parameter and show the decay of the energy for  $R = 25, 50, 80$  in Figure 12. We observe a very small window of time for which the larger values of  $R$  give a slower decay, but all the rates ultimately converge.

As in the previous tests, we are interested in comparing the rate of decay of the total energy corresponding to  $\gamma = 2$ . We compute the log of the total energy computed over the interval  $k \in [0, 50]$  letting  $t$  run to 100 seconds. This is plotted against the log of theoretical rate in Figure 13. The theoretical rate appears to be quite accurate in this case.

### 4.4 Test 4

Our last test also has periodic initial data

$$g_0(k) = \frac{k - 2n\pi}{2\pi} \quad k \in [2n\pi, 2(n+1)\pi), \quad (31)$$

for  $n \in \mathbb{N}_0$ . As in Test 3, we set  $\Delta k = 0.1$ ,  $T = 100$  and  $\Delta t = 0.0004$  when  $R = 25$  and  $R = 50$  but  $\Delta t = \frac{1}{4000}$  for  $R = 80$ .

We again give initial and final conditions in Figures 14a and 14b, respectively. As in Test 3, we observe that the energy is accumulated to a frequency near  $k = 0$  in some finite time  $T_s$ , where it remains with decaying  $L^\infty$  norm.

We let  $\gamma = 0, 1, 2$  and keep  $R = 50$  once again, and show the zeroth moments of these solutions in Figure 15. We again observe a slower decay for smaller values of  $\gamma$ .

Now fixing  $\gamma = 2$  once again, we see in Figure 16 that varying the truncation parameter has a similar result on the total energy as in the previous test cases. Note the scale of the x-axis.

Lastly, we give the log of the decay rate of the total energy corresponding to  $\gamma = 2$  plotted against the theoretical rate in Figure 17. The result is in good agreement with the theory.

## 5 Conclusions and Further Discussion

We introduce the first finite volume algorithm that allows to observe the long time asymptotics of the solutions of isotropic 3-wave kinetic equations, including the energy cascade behavior proved in [47]. Our numerical algorithm is based on the combination of the identity represented in Lemma 2.1 and Filbet-Laurençot's scheme [23] for the Smoluchowski coagulation equation.

From the four numerical tests, we can see that the energy cascade behavior happens for the case  $\gamma = 2$ , which was proved rigorously in [47]. At least for the initial data we consider, we observe that the energy cascade behavior could also happen for the case  $\gamma = 0, 1$ . Whether this is an accurate representation of true phenomenon for the continuous equation or this is simply misleading behavior due to the discretization is an open question to be proved rigorously.

From the solutions computed in sections 4.1, 4.2, 4.3, and 4.4, One can see that the smaller  $\gamma$  is, the slower the energy decays. The energy cascade behavior also seems to occur independently of the smoothness of the initial data for all four cases with  $\gamma = 0, 1, 2$ . We emphasize that, rigorously speaking, the case  $\gamma = 2$  has been proved in [47], while the two other cases are not yet proved.

In [47], it has been shown that the energy cascade rate is bounded by  $\mathcal{O}(\frac{1}{\sqrt{t}})$ . The numerical results confirm this theoretical bound and show that the decay rate should be  $\mathcal{O}(\frac{1}{t^s})$ , with  $s \in [\frac{1}{2}, 1]$  for various initial data. There is a case in which the decay rate is precisely  $\mathcal{O}(\frac{1}{\sqrt{t}})$ . We then conclude that the decay rate bound obtained in [47] is optimal.

We observe interesting behavior of the energy cascade that could be the subject of analysis in a follow-up work.

- (a) In Figure 2 and Figure 6, we observe that the yellow curve, indicating the higher moments for  $\gamma = 0$ , has a big jump when  $t$  is around some time  $t_0$ , and it lies above the red curves, indicating the higher moments for  $\gamma = 1$ , and the blue curves, indicating the higher moments for  $\gamma = 2$ , from that time on  $t > t_0$ , while the blue curve is still below the red curve at longer times. A deeper analysis needs to be done to understand this interesting phenomenon.
- (b) In all test cases, we observe for some  $T_s \in [0, T)$ , a large concentration of the remaining energy for  $k \in [0, R]$  is pushed toward  $k_s$  to some  $k_s > 0$ , then for  $t \in [T_s, \infty)$  the energy remains concentrated at  $k_s$  with decreasing  $L^\infty$  norm. This indicates the the energy decay happens in a very special way. We suspect that for an initial profile  $g_0$ ,

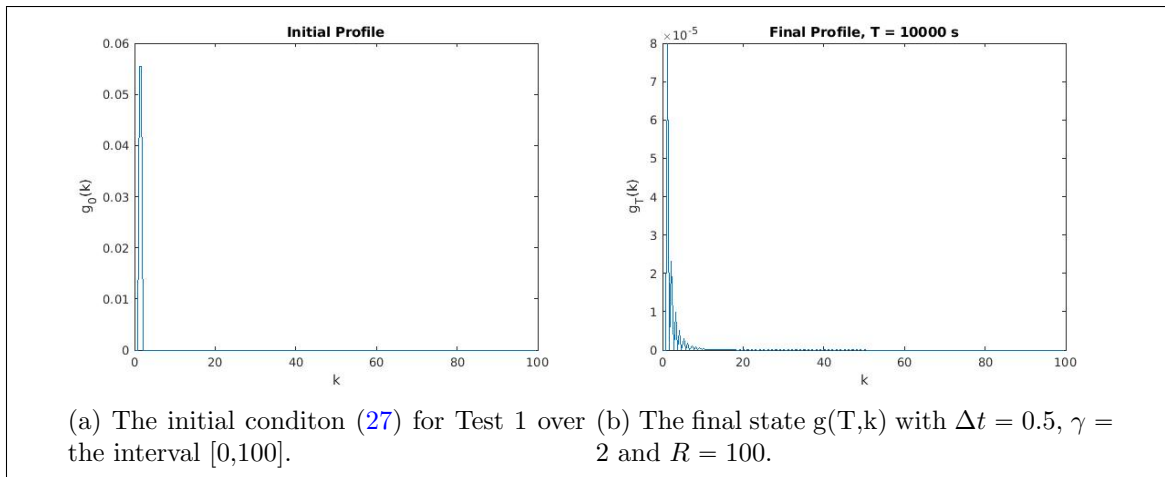


Figure 1

the energy over a finite interval converges to a self-similar configuration in finite time from which it decays to zero.

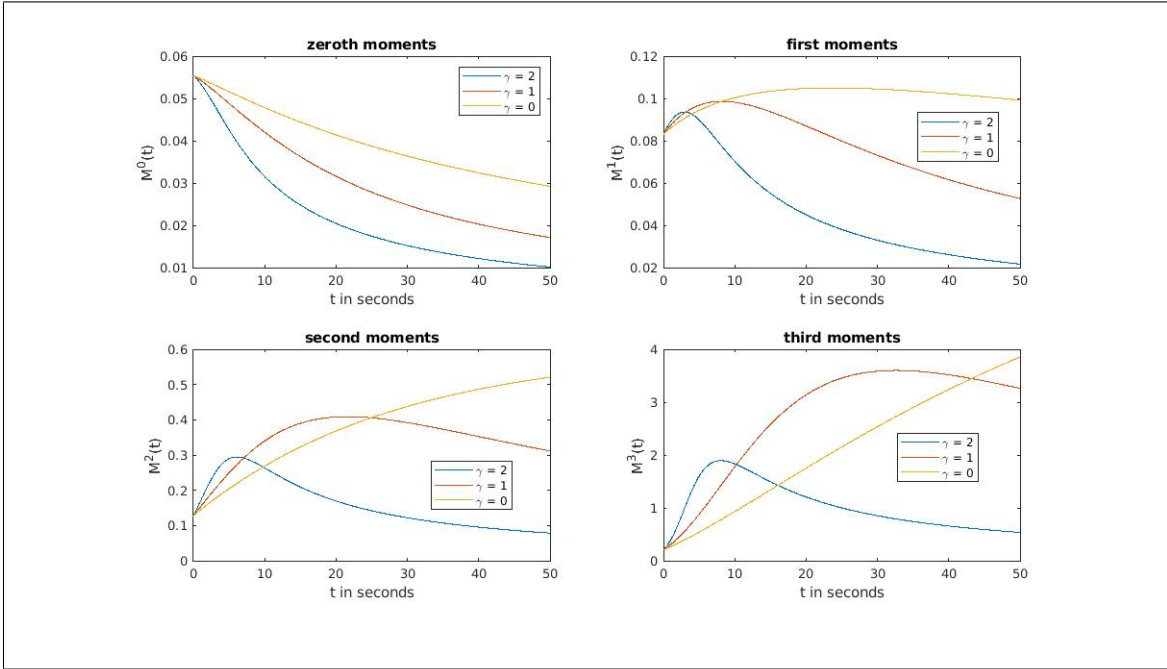


Figure 2: Here, we fix  $R = 100$  and compute the moments of the energy for  $\gamma = 0, 1, 2$  with initial condition (27).

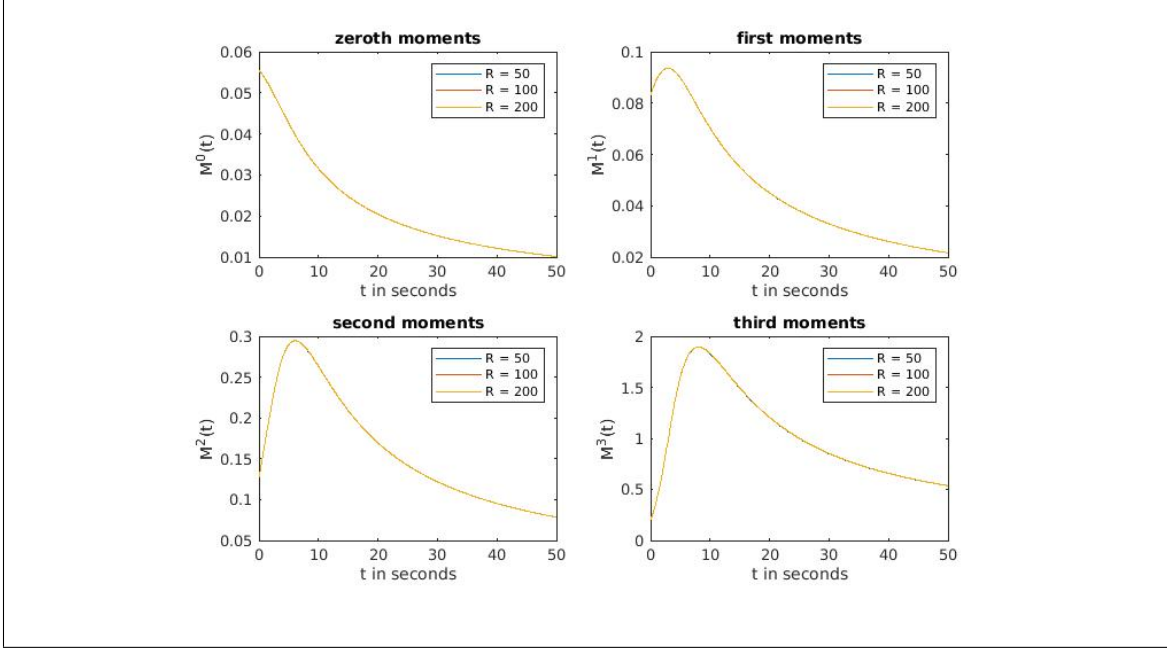


Figure 3: With  $\gamma = 2$  fixed, we compute the moments of the energy with initial condition (27) for truncation parameters  $R = 50, 100, 200$  with x-axis restricted to the interval  $[0, 50]$  for visual clarity.

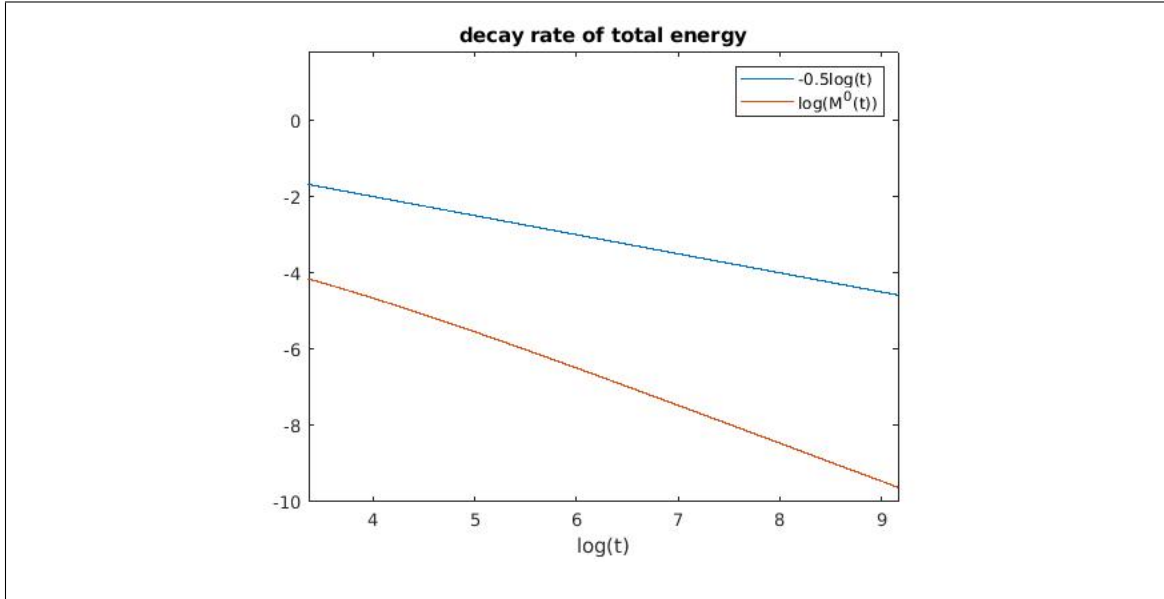


Figure 4: Rate of decay of the total energy,  $\int_{[0,R]} g(t, k) dk$ , corresponding to initial condition (27) with degree  $\gamma = 2$  fixed.

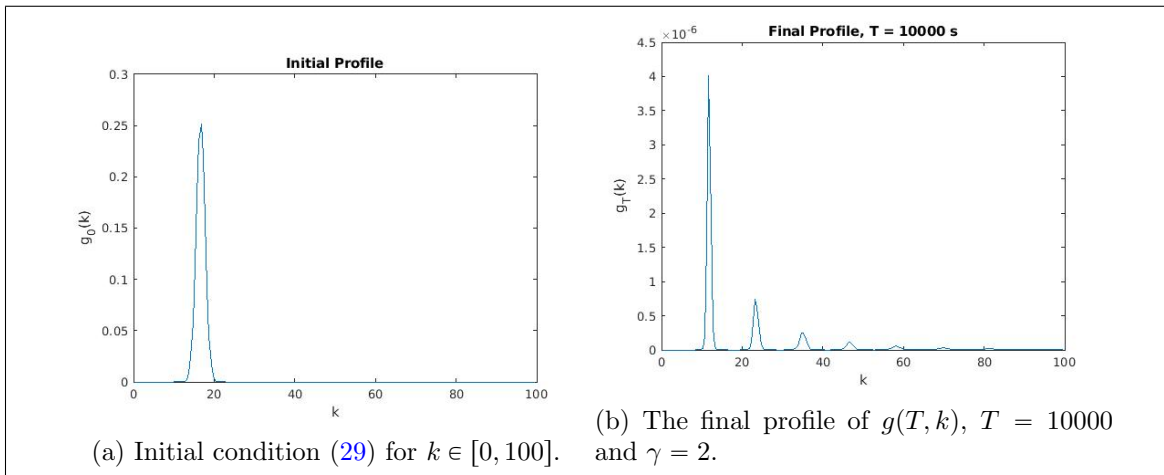


Figure 5

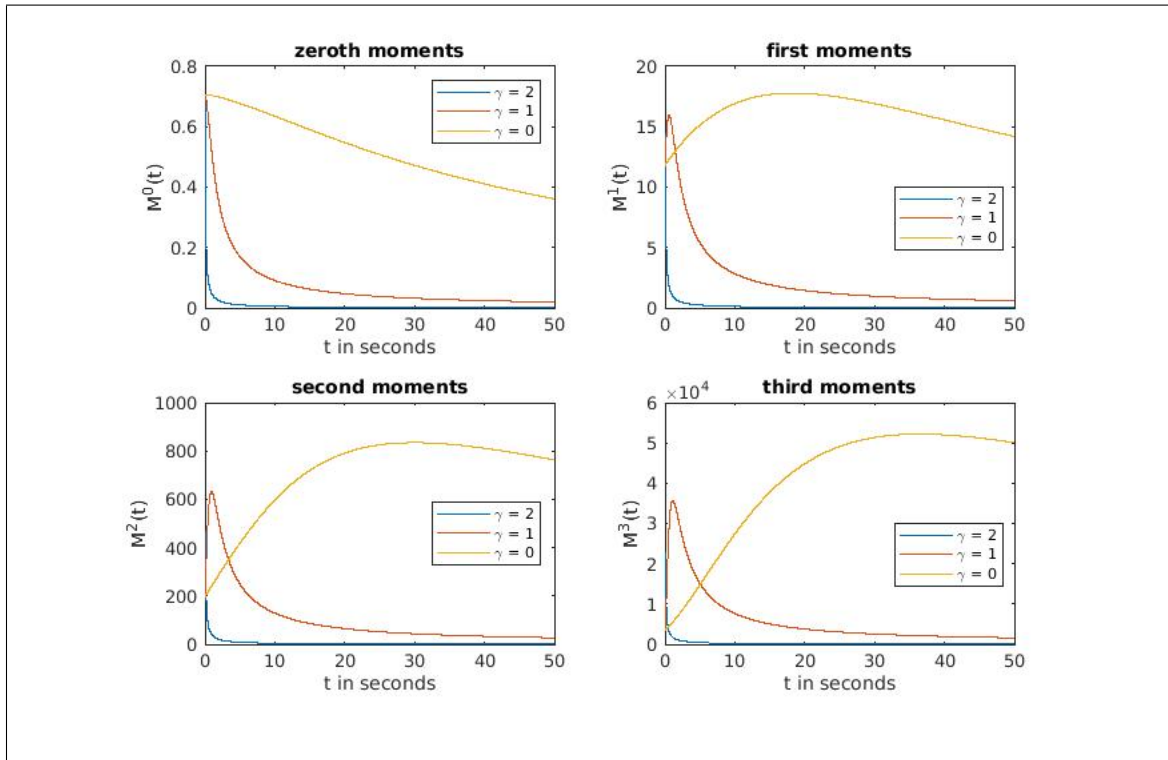


Figure 6: Moments of  $g(t, k)$  with initial condition (29) with fixed truncation parameter and varying degree. The x-axis is restricted for visibility.

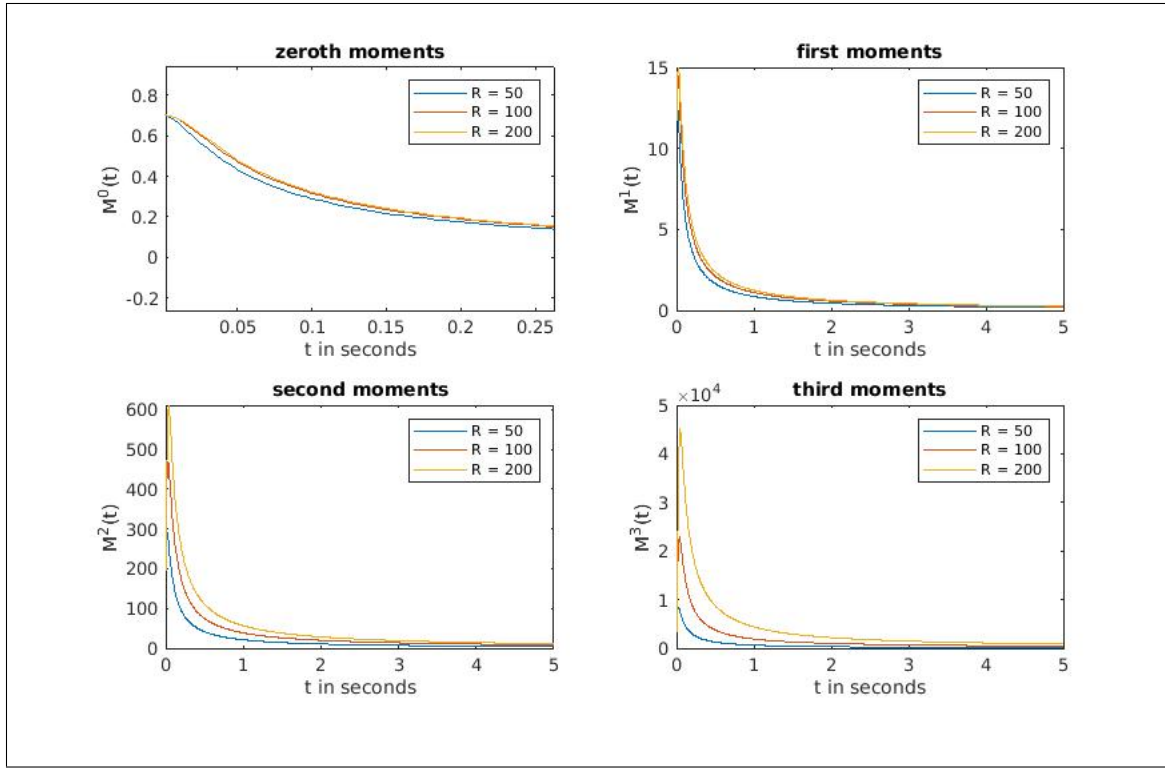


Figure 7: Moments of  $g(t, k)$  with initial condition (29) and fixed degree,  $\gamma = 2$ , and varying truncation parameter.

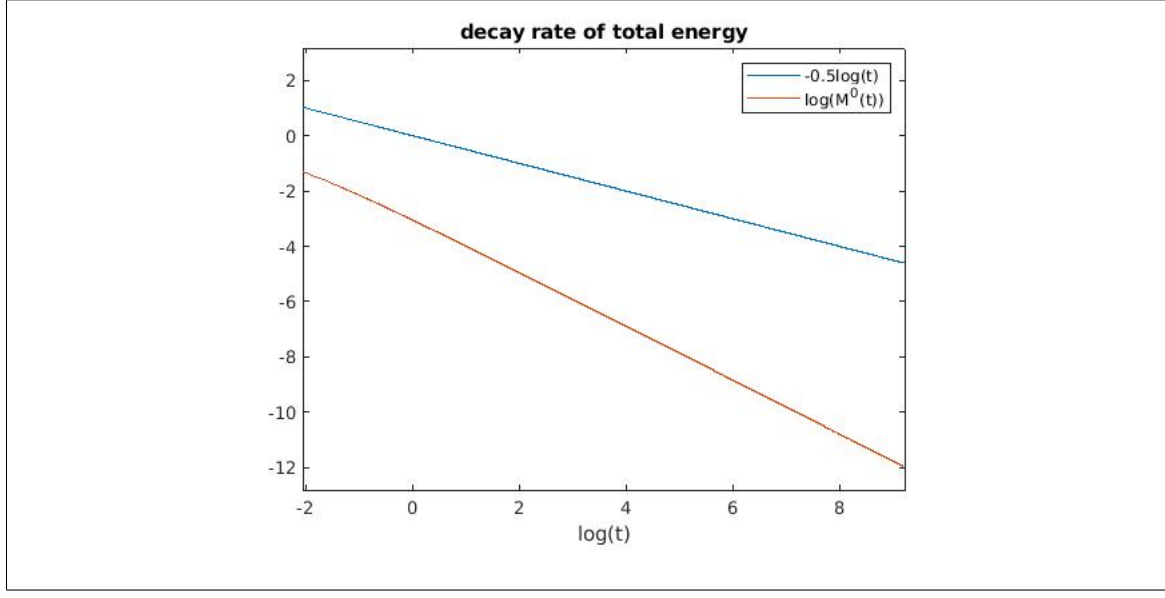


Figure 8: Rate of decay of the total energy,  $\int_{[0, R]} g(t, k) dk$ , corresponding to initial condition (29) with degree  $\gamma = 2$  fixed.

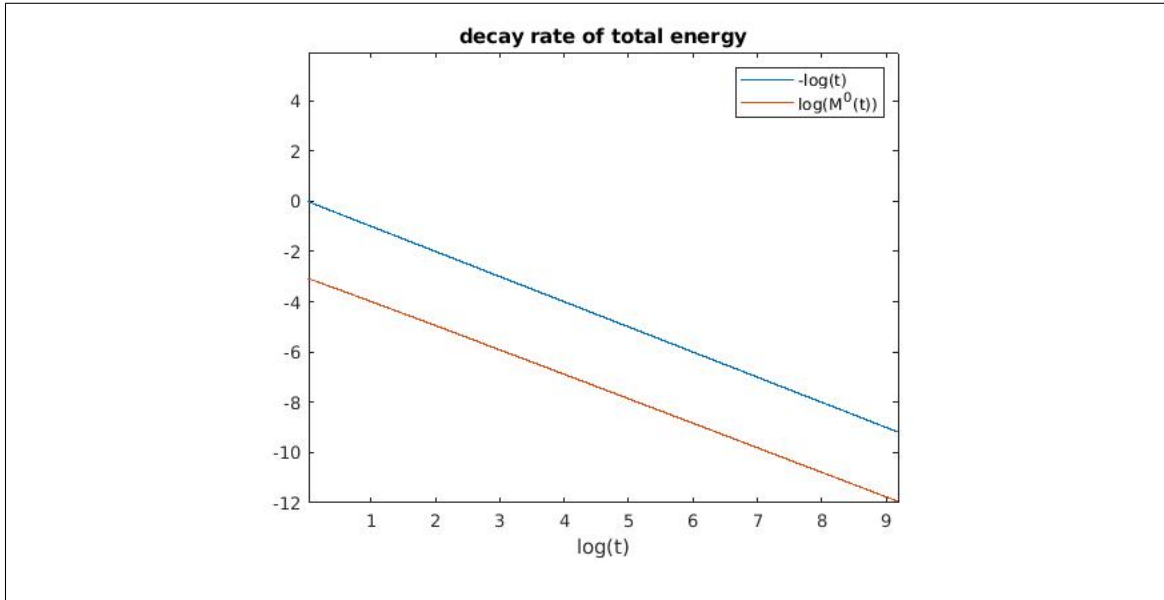


Figure 9: Rate of decay of the total energy, corresponding to initial condition (29) with degree  $\gamma = 2$  plotted against  $-\log(t)$ .

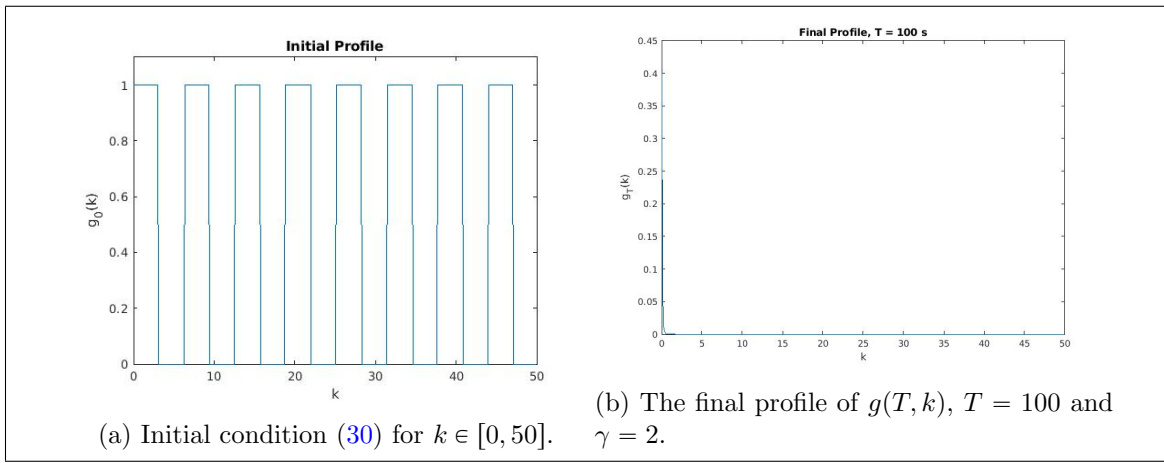


Figure 10

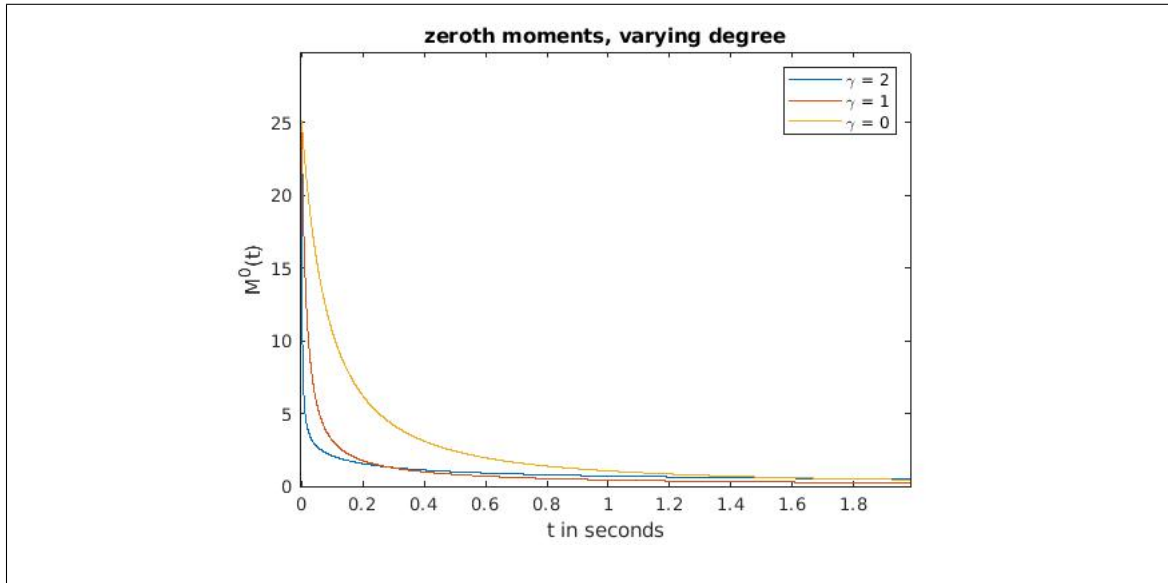


Figure 11: Zeroth moments of solution corresponding to initial condition 30, with  $R = 50$  and allowing  $\gamma$  to vary.

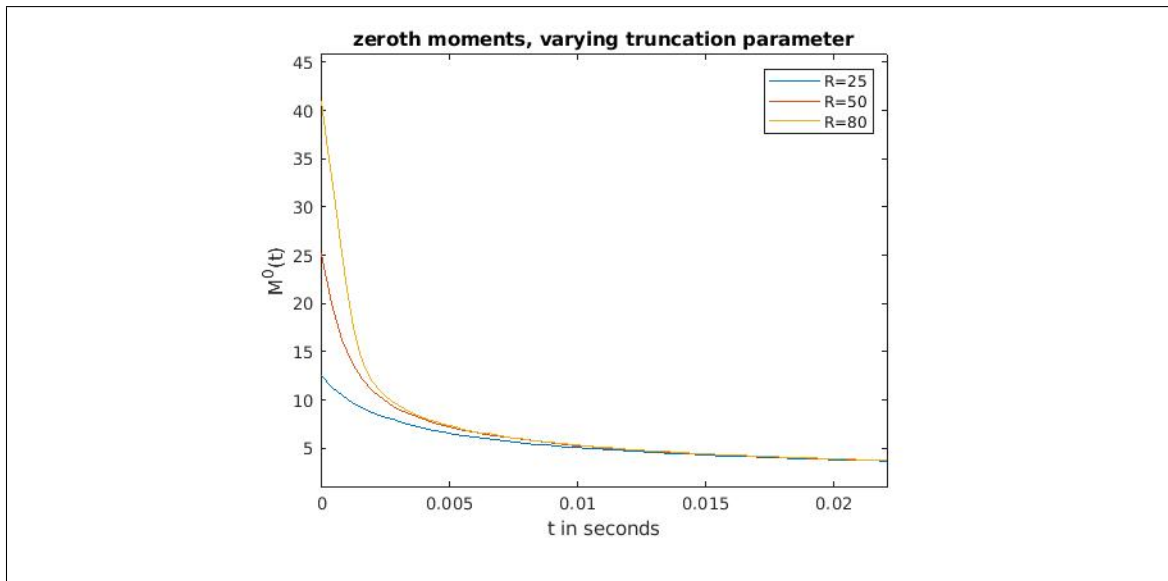


Figure 12: Zeroth moments of solution corresponding to initial condition 30, with  $\gamma = 2$  and allowing  $R$  to vary.

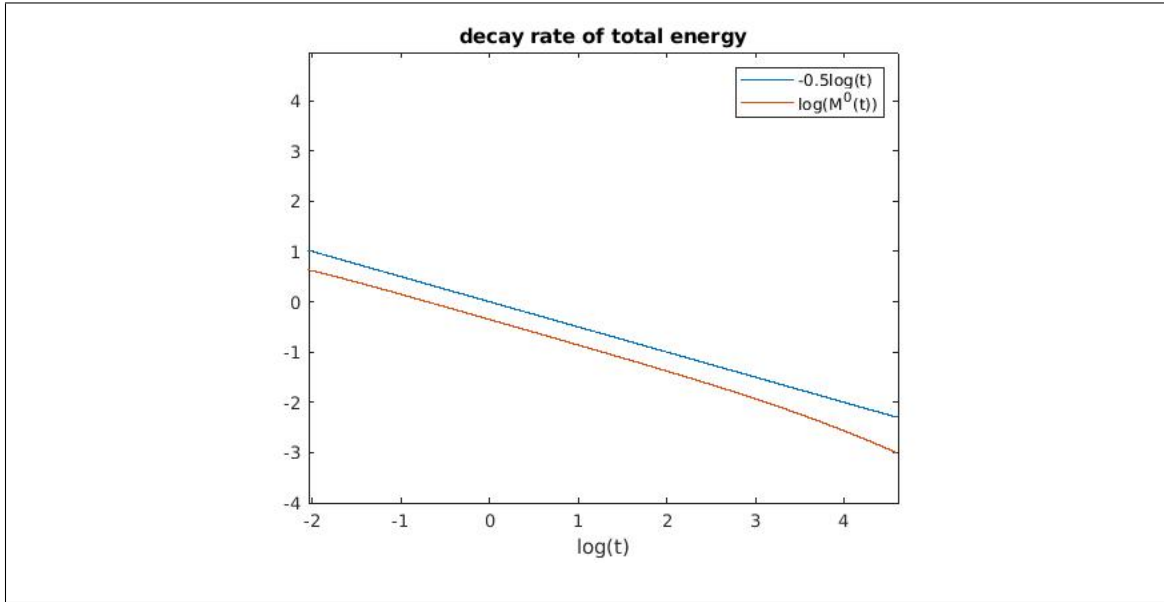


Figure 13: Log of the decay rate corresponding to  $\gamma = 2$  for initial condition 30 plotted against the log of theoretical rate.

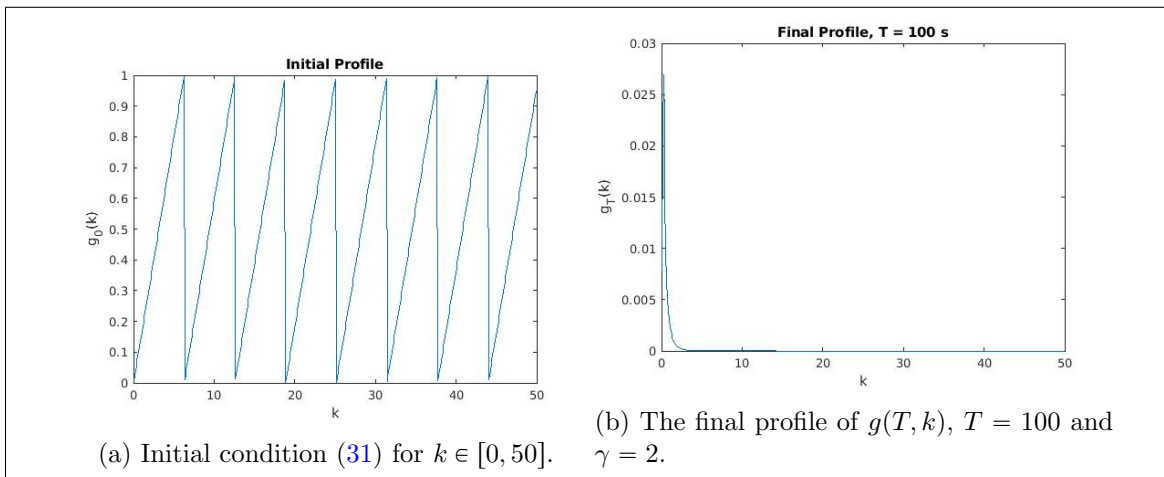


Figure 14

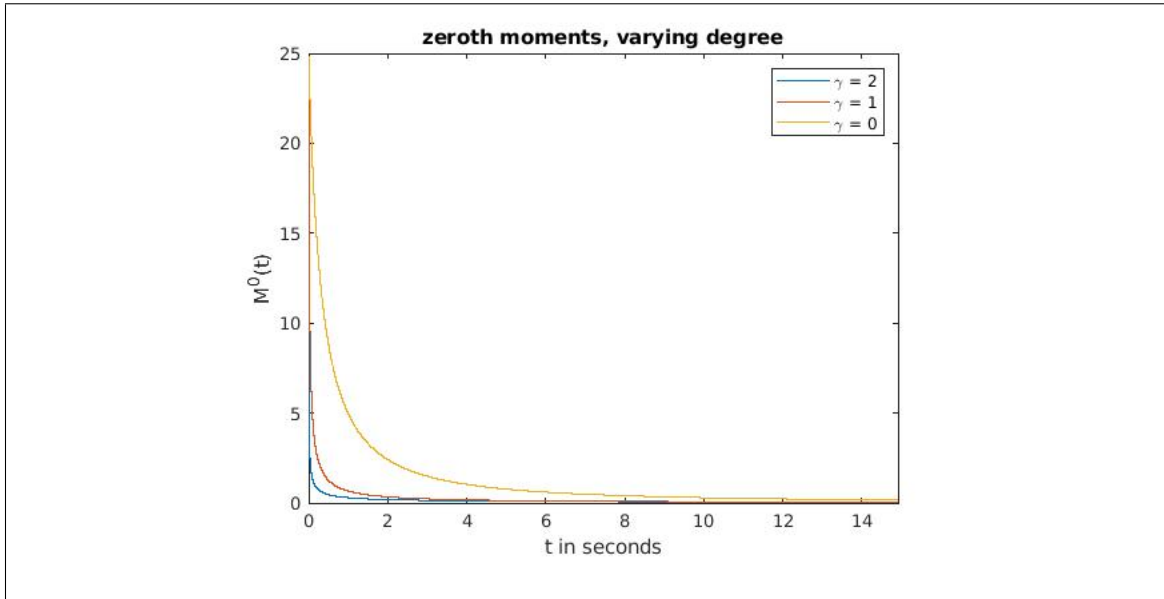


Figure 15: Zeroth moments of solution corresponding to initial condition 31, with  $R = 50$  and allowing  $\gamma$  to vary.

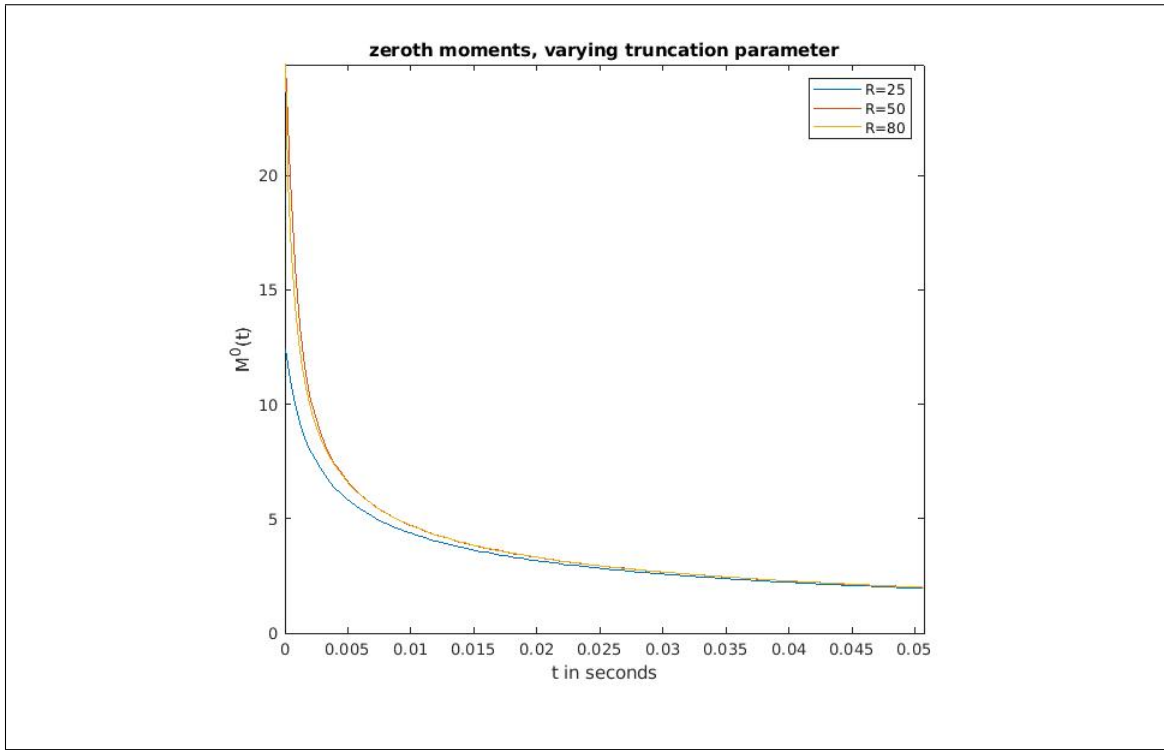


Figure 16: Zeroth moments of solution corresponding to initial condition 31, with  $\gamma = 2$  and allowing  $R$  to vary.

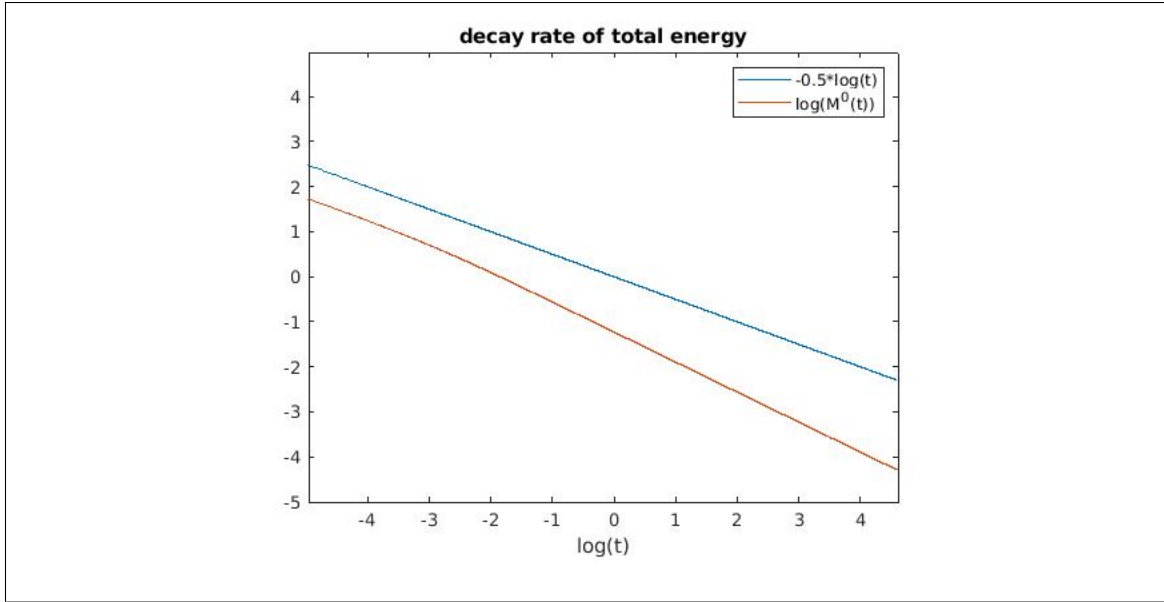


Figure 17: Log of the decay rate corresponding to  $\gamma = 2$  for initial condition 31.

## References

- [1] N. Alon, J. Bourgain, A. Connes, M. Gromov, and V. Milman, editors. *Visions in mathematics*. Modern Birkhäuser Classics. Birkhäuser Verlag, Basel, 2010. GAFA 2000 special volume. Part II, Papers from the Meeting “Visions in Mathematics—towards 2000” held at Tel Aviv University, Tel Aviv, August 25–September 3, 1999, Reprint [of MR1821865].
- [2] I. Ampatzoglou, C. Collot, and P. Germain. Derivation of the kinetic wave equation for quadratic dispersive problems in the inhomogeneous setting. *arXiv preprint arXiv:2107.11819*, 2021.
- [3] T. A. Bak and O. Heilmann. A finite version of smoluchowski’s coagulation equation. *Journal of Physics A: Mathematical and General*, 24(20):4889, 1991.
- [4] D. J. Benney and A. C. Newell. Random wave closures. *Studies in Applied Mathematics*, 48(1):29–53, 1969.
- [5] D. J. Benney and P. G. Saffman. Nonlinear interactions of random waves in a dispersive medium. *Proc. R. Soc. Lond. A*, 289(1418):301–320, 1966.
- [6] T. Buckmaster, P. Germain, Z. Hani, and J. Shatah. Analysis of the (CR) equation in higher dimensions. *International Mathematics Research Notices Accepted*, 2017.
- [7] T. Buckmaster, P. Germain, Z. Hani, and J. Shatah. Effective dynamics of the nonlinear schrödinger equation on large domains. *Communications on Pure and Applied Mathematics Accepted*, 2017.

- [8] J. Colliander, M. Keel, G. Staffilani, H. Takaoka, and T. Tao. Transfer of energy to high frequencies in the cubic defocusing nonlinear Schrödinger equation. *Invent. Math.*, 181(1):39–113, 2010.
- [9] C. Collot and P. Germain. On the derivation of the homogeneous kinetic wave equation. *arXiv preprint arXiv:1912.10368*, 2019.
- [10] C. Collot and P. Germain. Derivation of the homogeneous kinetic wave equation: longer time scales. *arXiv preprint arXiv:2007.03508*, 2020.
- [11] C. Connaughton. Numerical solutions of the isotropic 3-wave kinetic equation. *Physica D: Nonlinear Phenomena*, 238(23):2282–2297, 2009.
- [12] C. Connaughton and P. L. Krapivsky. Aggregation–fragmentation processes and decaying three-wave turbulence. *Physical Review E*, 81(3):035303, 2010.
- [13] C. Connaughton and A. C. Newell. Dynamical scaling and the finite-capacity anomaly in three-wave turbulence. *Physical Review E*, 81(3):036303, 2010.
- [14] F. P. Da Costa. A finite-dimensional dynamical model for gelation in coagulation processes. *Journal of nonlinear science*, 8(6):619–653, 1998.
- [15] Y. Deng and Z. Hani. On the derivation of the wave kinetic equation for nls. *arXiv preprint arXiv:1912.09518*, 2019.
- [16] Y. Deng and Z. Hani. Full derivation of the wave kinetic equation. *arXiv preprint arXiv:2104.11204*, 2021.
- [17] A. Dymov and S. Kuksin. Formal expansions in stochastic model for wave turbulence 1: kinetic limit. *arXiv preprint arXiv:1907.04531*, 2019.
- [18] A. Dymov and S. Kuksin. Formal expansions in stochastic model for wave turbulence 2: method of diagram decomposition. *arXiv preprint arXiv:1907.02279*, 2019.
- [19] A. Dymov and S. Kuksin. On the zakharov-l'vov stochastic model for wave turbulence. In *Doklady Mathematics*, volume 101, pages 102–109. Springer, 2020.
- [20] A. Dymov, S. Kuksin, A. Maiocchi, and S. Vladuts. The large-period limit for equations of discrete turbulence. *arXiv preprint arXiv:2104.11967*, 2021.
- [21] M. Escobedo and J. J. L. Velázquez. On the theory of weak turbulence for the nonlinear Schrödinger equation. *Mem. Amer. Math. Soc.*, 238(1124):v+107, 2015.
- [22] E. Faou, P. Germain, and Z. Hani. The weakly nonlinear large-box limit of the 2d cubic nonlinear schrödinger equation. *Journal of the American Mathematical Society*, 29(4):915–982, 2016.
- [23] F. Filbet and P. Laurençot. Numerical simulation of the smoluchowski coagulation equation. *SIAM Journal on Scientific Computing*, 25(6):2004–2028, 2004.

- [24] S. Galtier, S. V. Nazarenko, A. C. Newell, and A. Pouquet. A weak turbulence theory for incompressible magnetohydrodynamics. *Journal of Plasma Physics*, 63(5):447–488, 2000.
- [25] I. M. Gamba, L. M. Smith, and M.-B. Tran. On the wave turbulence theory for stratified flows in the ocean. *M3AS: Mathematical Models and Methods in Applied Sciences. Vol. 30, No. 1* 105-137, 2020.
- [26] P. Germain, Z. Hani, and L. Thomann. On the continuous resonant equation for NLS, II: Statistical study. *Analysis & PDE*, 8(7):1733–1756, 2015.
- [27] P. Germain, Z. Hani, and L. Thomann. On the continuous resonant equation for NLS. I. Deterministic analysis. *Journal de Mathématiques Pures et Appliquées*, 105(1):131–163, 2016.
- [28] K. Hasselmann. On the non-linear energy transfer in a gravity-wave spectrum part 1. general theory. *Journal of Fluid Mechanics*, 12(04):481–500, 1962.
- [29] K. Hasselmann. On the spectral dissipation of ocean waves due to white capping. *Boundary-Layer Meteorology*, 6(1-2):107–127, 1974.
- [30] X. Y. Hu, N. A. Adams, and C.-W. Shu. Positivity-preserving method for high-order conservative schemes solving compressible euler equations. *Journal of Computational Physics*, 242:169–180, 2013.
- [31] J. Huang and C.-W. Shu. Positivity-preserving time discretizations for production–destruction equations with applications to non-equilibrium flows. *Journal of Scientific Computing*, 78(3):1811–1839, 2019.
- [32] J. Huang, W. Zhao, and C.-W. Shu. A third-order unconditionally positivity-preserving scheme for production–destruction equations with applications to non-equilibrium flows. *Journal of Scientific Computing*, 79(2):1015–1056, 2019.
- [33] B. B. Kadomtsev. Plasma turbulence. *New York: Academic Press*, 1965, 1965.
- [34] D. D. Keck and D. M. Bortz. Numerical simulation of solutions and moments of the smoluchowski coagulation equation. *arXiv preprint arXiv:1312.7240*, 2013.
- [35] A. O. Korotkevich, A. I. Dyachenko, and V. E. Zakharov. Numerical simulation of surface waves instability on a homogeneous grid. *Phys. D*, 321/322:51–66, 2016.
- [36] G. Laibe and M. Lombart. On the courant-friedrichs-lewy condition for numerical solvers of the coagulation equation. *arXiv preprint arXiv:2109.11065*, 2021.
- [37] J. Lukkarinen and H. Spohn. Weakly nonlinear Schrödinger equation with random initial data. *Invent. Math.*, 183(1):79–188, 2011.
- [38] Y. V. Lvov, K. L. Polzin, E. G. Tabak, and N. Yokoyama. Oceanic internal-wave field: theory of scale-invariant spectra. *Journal of Physical Oceanography*, 40(12):2605–2623, 2010.

[39] R. Micha and I. I. Tkachev. Turbulent thermalization. *Physical Review D*, 70(4):043538, 2004.

[40] T. T. Nguyen and M.-B. Tran. On the Kinetic Equation in Zakharov's Wave Turbulence Theory for Capillary Waves. *SIAM J. Math. Anal.*, 50(2):2020–2047, 2018.

[41] R. Peierls. Zur kinetischen theorie der warmeleitung in kristallen. *Annalen der Physik*, 395(8):1055–1101, 1929.

[42] R. E. Peierls. Quantum theory of solids. In *Theoretical physics in the twentieth century (Pauli memorial volume)*, pages 140–160. Interscience, New York, 1960.

[43] Y. Pomeau and M.-B. Tran. Statistical physics of non equilibrium quantum phenomena. *Lecture Notes in Physics, Springer*, 2019.

[44] A. N. Pushkarev and V. E. Zakharov. Turbulence of capillary waves. *Physical review letters*, 76(18):3320, 1996.

[45] A. N. Pushkarev and V. E. Zakharov. Turbulence of capillary waves: theory and numerical simulation. *Physica D: Nonlinear Phenomena*, 135(1):98–116, 2000.

[46] B. Rumpf, A. Soffer, and M.-B. Tran. On the wave turbulence theory: ergodicity for the elastic beam wave equation. *arXiv preprint arXiv:2108.13223*, 2021.

[47] A. Soffer and M.-B. Tran. On the energy cascade of 3-wave kinetic equations: beyond kolmogorov–zakharov solutions. *Communications in Mathematical Physics*, pages 1–48, 2019.

[48] G. Staffilani and M.-B. Tran. On the wave turbulence theory for stochastic and random multidimensional kdv type equations. *arXiv preprint arXiv:2106.09819*, 2021.

[49] M.-B. Tran, G. Craciun, L. M. Smith, and S. Boldyrev. A reaction network approach to the theory of acoustic wave turbulence. *Journal of Differential Equations*, 269(5):4332–4352, 2020.

[50] V. E. Zakharov. Weak turbulence in media with a decay spectrum. *Journal of Applied Mechanics and Technical Physics*, 6(4):22–24, 1965.

[51] V. E. Zakharov. Stability of periodic waves of finite amplitude on the surface of a deep fluid. *Journal of Applied Mechanics and Technical Physics*, 9(2):190–194, 1968.

[52] V. E. Zakharov and N. N. Filonenko. Weak turbulence of capillary waves. *Journal of applied mechanics and technical physics*, 8(5):37–40, 1967.

[53] V. E. Zakharov, V. S. L'vov, and G. Falkovich. *Kolmogorov spectra of turbulence I: Wave turbulence*. Springer Science & Business Media, 2012.

[54] V. E. Zakharov and S. V. Nazarenko. Dynamics of the Bose-Einstein condensation. *Phys. D*, 201(3-4):203–211, 2005.